A Cell-Free Approach Based on Phospholipid Characterization for Determination of the Cell Specific Unbound Drug Fraction (f$_{u,cell}$)

Andrea Treyer[1] • Sandra Walday[1] • Hinnerk Boriss[2] • Pär Matsson[1] • Per Artursson[1,3,4]

ABSTRACT

Purpose The intracellular fraction of unbound compound (f$_{u,cell}$) is an important parameter for accurate prediction of drug binding to intracellular targets. f$_{u,cell}$ is the result of a passive distribution process of drug molecules partitioning into cellular structures. Initial observations in our laboratory showed an up to 10-fold difference in the f$_{u,cell}$ of a given drug for different cell types. We hypothesized that these differences could be explained by the phospholipid (PL) composition of the cells, since the PL cell membrane is the major sink of unspecific drug binding. Therefore, we determined the f$_{u,cell}$ of 19 drugs in cell types of different origin.
Method The cells were characterized for their total PL content and we used mass spectrometric PL profiling to delineate the impact of each of the four major cellular PL subspecies: phosphatidylcholine (PC), phosphatidylethanolamine (PE), phosphatidylserine (PS) and phosphatidylinositol (PI). The cell-based experiments were compared to cell-free experiments that used beads covered by PL bilayers consisting of the most abundant PL subspecies.
Results PC was found to give the largest contribution to the drug binding. Improved correlations between the cell-based and cell-free assays were obtained when affinities to all four major PL subspecies were considered. Together, our data indicate that f$_{u,cell}$ is influenced by PL composition of cells.
Conclusion We conclude that cellular PL composition varies between cell types and that cell-specific mixtures of PLs can replace cellular assays for determination of f$_{u,cell}$ as a rapid, small-scale assay covering a broad dynamic range.

KEY WORDS cell-free assays · intracellular bioavailability · phospholipid membranes · unbound drug fraction

ABBREVIATIONS

A549	Adenocarcinomic human alveolar basalepithelial cells
Caco-2	Human epithelial colorectal adenocarcinoma cells
DMEM	Dulbecco's Modified Eagle's Medium
FBS	Fetal bovine serum
f$_{u,cell}$	Intracellular fraction of unbound compound
HEK293	Human embryonic kidney 293 cells
HH	Human hepatocytes
HL-60	Human leukemia cell line
K562	Myelogenous leukemia cells derived from bone marrow
LLC-PK1	Lilly Laboratories Cell-Porcine Kidney 1
logD$_{7.4}$	Octanol-buffer distribution coefficient at pH 7.4
MDCK	Madin-Darby canine kidney cells
MW	Molecular weight
PA	Phosphatidic acid
PC	Phosphatidylcholine
PCA	Principal component analysis
PE	Phosphatidylethanolamine
PEST	Penicillin-streptomycin
PG	Phosphatidylglycerol
PI	Phosphatidylinositol

✉ Per Artursson
per.artursson@farmaci.uu.se

[1] Department of Pharmacy, Uppsala University, Box 580, SE-751 23 Uppsala, Sweden

[2] HBO consult GmbH, 04155 Leipzig, Germany

[3] Science for Life Laboratory Drug Discovery and Development platform (SciLifelab DDD-P), Uppsala, Sweden

[4] Uppsala University Drug Optimization and Pharmaceutical Profiling Platform (UDOPP), Uppsala University, Uppsala, Sweden

PL	Phospholipid
PS	Phosphatidylserine
PSA	Polar surface area
RMSE	Root mean square error

INTRODUCTION

Determination of intracellular unbound drug concentrations has gained importance over the last decade [1,2]. Several techniques for determination of the intracellular unbound drug accumulation ratio at steady-state (Kp_{uu}) or intracellular bio-availability (F_{ic}) have been published recently and have been summarized by the international transporter consortium [3]. Many of the techniques determine the total accumulation ratio at equilibrium (Kp) and the fraction unbound to cells ($f_{u,cell}$), which are combined to calculate Kp_{uu} or F_{ic}. Kp is generally determined by performing drug uptake experiments in suspended or plated cells. The most prominent techniques for determining $f_{u,cell}$ are the binding/homogenization method, temperature method, or predictions from $logD_{7.4}$ [1,4].

Mechanisms such as active and passive transport processes across cell membranes, as well as partitioning into substructures of the cell (e.g., lysosomal trapping) are relatively well understood. However, the subcellular structures that determine $f_{u,cell}$ have not been investigated in detail. The current study investigates previously observed differences of $f_{u,cell}$ between different cell types. More specifically, we observed a lower $f_{u,cell}$ in human hepatocytes than in HEK293 cells, consistent with an approximately 5-fold greater binding capacity of the former, but we did not identify the factors behind this difference [5]. More recently, we showed that induction of the phospholipid (PL) content in 3T3-L1 cells results in a corresponding increase in drug binding. In contrast, no increase in $f_{u,cell}$ was observed after a 5-fold enhancement of the cellular content of neutral lipids [6]. Global quantitative proteomics analysis allowed us to investigate the relative importance of intracellular drug binding proteins such as fatty acid binding proteins. These comparisons show that PLs are the major sink for unspecific drug binding, and dominate over protein binding [6]. PL membranes are complex structures, and little is known about the binding mechanisms of drugs towards the different PL subtypes.

In the present study, we therefore compared the $f_{u,cell}$ of 19 chemically diverse drugs in cell types derived from different tissues (lung, intestine, liver, kidney, blood, and bone marrow). We next determined the PL composition in each of the cell types by mass spectrometric PL profiling. We then constructed beads covered with PL membranes, consisting of single PL subspecies as well as a PL-mixture, to represent the membrane of a prototypical cell. This allowed us to determine the contribution of each PL subspecies to cellular drug binding separately. The $f_{u,cell}$ values were then compared to binding affinities measured with the bead-immobilized membranes of defined PL composition. We speculated that a PL-based cell-free assay that could predict $f_{u,cell}$ and still take the cell specific lipid composition into account would provide an advantage over the current cell-based methodology. Moreover, membrane dialysis can be a limiting step for very large or very lipophilic compounds that cannot pass the pores in the dialysis membrane. A better understanding of the influence of different cellular constituents on $f_{u,cell}$ would enable the development of alternative methods that overcome these challenges.

MATERIALS AND METHODS

Chemicals

Compounds were purchased from Fluka (caffeine, phenazopyridine), Baxter (esmolol), Therapeutic Research Center (fluconazole) or Sigma Aldrich (remaining compounds) at their highest available purity (>95%). The compounds were dissolved at a concentration of 10 mM in DMSO or at their highest possible solubility if lower. DMSO stocks were kept at −20°C.

Compound Selection

Compounds were selected to represent the common chemical space of small-molecule drugs, based on a principal component analysis of 334 ADME-related molecular properties using ADMET predictor (Simulations Plus, version 7.2), as described elsewhere [6]. The final compound set comprised compounds representing all charge classes and with molecular weight (MW), polar surface area (PSA) and lipophilicity ($logD_{7.4}$) ranging from 194 to 629, 28 to 146 Å and − 0.7 to 5.0, respectively (Table S1).

Cell Culture

Cells were grown in T75 culture flasks at 37°C and 5% CO_2 atmosphere (10% for Caco-2 cells) and passaged and/or harvested at 80-100% confluency. Suspended cells were maintained at a cell density between 1×10^5 and 1×10^6 viable cells/ml. HEK293 and A549 cells were grown in Dulbecco's Modified Eagle's Medium (DMEM) supplemented with 10% fetal bovine serum (FBS), 1% penicillin-streptomycin (PEST) and 2 mM L-glutamine. MDCK cells were grown in DMEM supplemented with 10% FBS, 1% PEST and 1% Glutamax. LLC-PK1 cells were grown in medium 199 supplemented with 10% FBS, 1% PEST and 2 mM L-glutamine. K562 and HL60 cells were grown in Roswell Park Memorial Institute (RPMI) 1640 medium supplemented with 10% FBS, 1% PEST and 2 mM L-glutamine and Caco-2 in

DMEM supplemented with 10% FBS and 1% nonessential amino acids. After trypsinisation, cells were pelleted at 10-30 million cells per flask and stored at −20°C until further processing. Primary human hepatocytes (HH) were frozen directly after isolation from human liver tissue using a two-step collagenase procedure as described elsewhere (7,8). Ethical approval was granted by the Uppsala Regional Ethics Committee (ethical approvals no. 2009/028 and 2011/037).

Determination of $f_{u,cell}$

$f_{u,cell}$ was measured in cassette-mode as previously described with minor modifications (9). Briefly, 10 million cells/mL were suspended in HBSS buffered with 10 mM HEPES and homogenized on ice by sonication (VCX 750 Sonicator, 3 mm probe, 20% intensity, 10 s). Up to 8 compounds were combined randomly and spiked into the homogenate for a final concentration of 0.5 µM. Equilibrium dialysis was performed in a Rapid Equilibrium device (Thermo Fisher Scientific) against blank HBSS buffered with 10 mM HEPES, for 4 h at 37°C on an orbital shaker at 900 rpm. Stability controls were kept at 4° and 37°C for the duration of the experiment. The concentration in both dialysis chambers was quantified by extracting the compound with acetonitrile/water (60/40) containing internal standard. Matrixes were matched with blank buffer or cell homogenate, respectively. LC-MS/MS parameters are available in Table S9. All experiments were carried out in triplicates and at least at two independent occasions.

The unbound fraction in the cell homogenate ($f_{u,hom}$) was determined according to Eq. (1):

$$f_{u,hom} = \frac{C_{buffer}}{C_{hom}} \tag{1}$$

and the fraction of unbound compound in the cell ($f_{u,cell}$) was calculated by correcting for homogenate dilution according to Eq. (2):

$$f_{u,cell} = \frac{1}{D_P \cdot \left(1/f_{u,hom} - 1 \right) + 1} \tag{2}$$

where the dilution constant D_P was calculated using Eq. (3), assuming the V_{cell} to be equal to 6.5 µL/mg protein (6,10). Protein content in the cell homogenates was determined at each experiment using the BCA Protein Assay Reagent Kit (Thermo Fisher Scientific Inc.).

$$D_P = 1/V_{cell} \tag{3}$$

Determination of $f_{u,PL}$

$f_{u,PL}$ was derived from membrane affinity measurements to beads covered with PLs as previously described (6). PL-covered silica beads with PC (Sovicell, Transil Absorption Kit, No. TMP-0100-2096), PE (no. TMP-0130-2096), PS (no. TMP-0140-2096) or PE/PS/PI/PC (21.6/12/14.3/52.1 mol%) (no. TMP-0150-2096) were used to determine membrane affinity, defined as (4)

$$membrane\ affinity = \frac{C_{membrane}}{C_{buffer}} \tag{4}$$

C_{buffer} was quantified by LC-MS/MS in samples of the supernatant that was obtained after 15 min incubation time on an orbital shaker at 1000 rpm and subsequent separation from the beads by centrifugation at 750 x g. $C_{membrane}$ was calculated taking into account the volume of the lipid membrane (90 µl) using the provided software from the Absorption Kit (TMP-0100-2096) and the mass balance equation:

$$n = c_b \cdot V_b + c_m \cdot V_m \tag{5}$$

where n: total amount of drug, c: concentration, V: volume, b: buffer, m: membrane. Unspecific binding was evaluated by incubations into wells without added lipids.

Finally, $f_{u,PL}$ was derived as follows:

$$f_{u,PL} = \frac{C_{buffer}}{C_{buffer} + C_{membrane}} \tag{6}$$

Prediction of $f_{u,hom}$

$f_{u,hom,pred}$ was calculated by scaling $f_{u,PL}$ from the pure PL system to the homogenates, applying an optimized dilution factor (D_L) determined by minimizing the sum of the squared prediction errors (Microsoft Excel, Solver add-in, version 16.0):

$$f_{u,hom,pred} = \frac{1}{D_L \cdot \left(1/f_{u,PL} - 1 \right) + 1} \tag{7}$$

Phospholipid Content in Cell Homogenates

The PL content of cell homogenates was quantified using the enzymatic-colorimetric WAKO LabAssay Phospholipid Choline Oxidase/DAOS method (Nordic Biolabs) according to the manufacturer's instructions. Briefly, 2 µl of the cell homogenate and the provided standards were deposited in a 96-well black, clear-bottom plate and 300 µl of colour reagent was added prior to incubation at 37°C for 5 min. Absorbance was measured for multiple reads per well at 600 nm in a plate reader.

ESI-MS/MS Based Quantification of Phospholipid Subspecies

Proportional content of the PL subspecies was determined using a shotgun lipidomic approach. The lipids were extracted

from the cellular homogenates by a liquid-liquid extraction. This extraction method, using methyl-*tert*-butyl ether (MTBE) as organic solvent, gives recoveries of approximately 90% for several PL subspecies (11). Cell pellets were suspended at 50 million cells per ml and homogenized by sonication (VCX 750 Sonicator, 3 mm probe, 20% intensity, 10 s). The sample (500 µL) was transferred to a glass vial to which 1800 µL of high-grade methanol was added. After vortexing, 6 ml of MTBE was added, and the samples were shaken on an orbital shaker at 600 rpm for 1 h. Phase separation was induced by adding 1250 µL of purified water. After 5 min, the samples were centrifuged for 10 min at 1000x *g* and the upper organic phase was separated using a glass pipette. The sample was re-extracted by adding artificial organic phase (MTBE:methanol:water at 4:1.2:1, *v/v/v*) to the water phase. After pooling the organic phases from both steps together, the solvent was evaporated on a vacuum centrifuge (EZ-2 MK2 Plus centrifugal evaporator, Genevac Ltd., Ipswich, England). Samples were stored under inert atmosphere at −80°C if not processed immediately. For MS analysis, the samples were dissolved in 200 µL analysis buffer consisting of isopropanol, methanol and water (5:1:4, *v/v/v*) containing 0.2% (v/v) formic acid and 0.028% (*w/v*) ammonium acetate (12).

For mass-spectrometry based PL profiling, mixtures were further diluted 1:1000 in analysis buffer and infused at a flow rate of 0.1 ml/min into the ion source of a Sciex QTRAP 6500 mass spectrometer using a glass syringe. Spectra of specific fragments of each PL subspecies were acquired simultaneously, using precursor ion scan (184 Da m/z for PC and SM) or neutral loss scan (141 Da m/z for PE, 185 Da m/z for PS, 98 Da m/z for PA, 277 Da m/z for PI and 172 Da m/z for PG) in positive mode (13,14). Ion intensities were exported from Analyst 1.6.2 software (AB Sciex, Framingham, MA, USA), then summed up and normalized against intensities from a standard of known concentration for each subspecies of PLs (the mixture came from the Differential Ion Mobility System Suitability LIPIDOMIX kit, no. 330708, Avanti, Alabama, USA).

Calculation of Molecular Properties

Chemical structures of the study compounds were accessed from DrugBank (15) or PubChem (http://pubchem.ncbi.nlm.nih.gov) in SMILES format. Three-dimensional structures were generated using Corina (Molecular Networks, version 4.1) and were used as input for molecular property calculations using the ADMET Predictor (Simulations Plus, version 7.2).

Statistical Analysis

All statistical analyses were performed in Graph-Pad Prism (version 7.04). R^2 and root-mean square error (RMSE) were calculated using the linear regression function. For correlations between lipid content and $f_{u,cell}$, the slope of the linear regression was considered significantly non-zero at a *p* value <0.05. $f_{u,cell}$ experiments were carried out in triplicates and were performed on at least two independent occasions.

RESULTS

Comparison of $f_{u,cell}$ between Cell Types

The fraction of unbound drug in cells ($f_{u,cell}$) was determined in six cell types originating from different human tissues (Fig. 1a) using equilibrium dialysis of drug added to cell homogenates, as described previously (5,16). In addition, LLC-PK1 cells derived from pig kidney and MDCK cells from dog kidney (proximal and distal tubular epithelium, respectively) were included for inter-species comparison. $f_{u,cell}$ was first determined for 19 structurally diverse drugs (Fig. 1b, Table S1 and Fig. S2). The drug selection was based on a principal component analysis (PCA) using 1146 drugs and 334 predicted ADMET-related molecular properties (Fig. 1b), to assure that a wide range of physico-chemical properties were covered (MW: 194 to 629, PSA: 28 to 146 Å, $logD_{7.4}$, −0.7 to 5.0; Table S1) (6).

The $f_{u,cell}$ values, determined using membrane equilibrium dialysis, spanned four orders of magnitude and followed a similar pattern for all cell types, but with an average 9.3-fold difference between the maximum and minimum values for the different cell types (Fig. 1c). In general, the highest $f_{u,cell}$-values were observed in the HL60 and K562 cell lines and the lowest $f_{u,cell}$-values in HH. For all cell types, $f_{u,cell}$ was related to the lipophilicity of the compounds, and the geometric mean values of $f_{u,cell}$ across all cell types were negatively correlated to the logD values ($R^2 = 0.65$; Fig. 1d) (5). No correlation was observed between $f_{u,cell}$ and $f_{u,plasma}$ (15) (Fig. 1e). In the three kidney-derived cell lines (HEK293, LLC-PK1 and MDCK), the variation between cell types was, on average, lower (Fig. S3). When the two renal epithelia cell lines (LLC-PK1 and MDCK) were compared with each other, the average difference was further reduced to 1.8-fold.

$f_{u,cell}$ in Comparison to Total Phospholipid Content in Cells

We previously observed a decrease in $f_{u,cell}$ with increased PL content in the mouse fibroblast 3T3-L1 cell line (6). We hypothesized that the difference in binding between unrelated cell types could also be explained by differences in total PL content. For this purpose, we first determined total PL content per cell using an enzymatic kit and sorted the six cell types in descending order (Fig. 2a). Total PL content was then related to the median $f_{u,cell}$ across the six cell types. Statistical
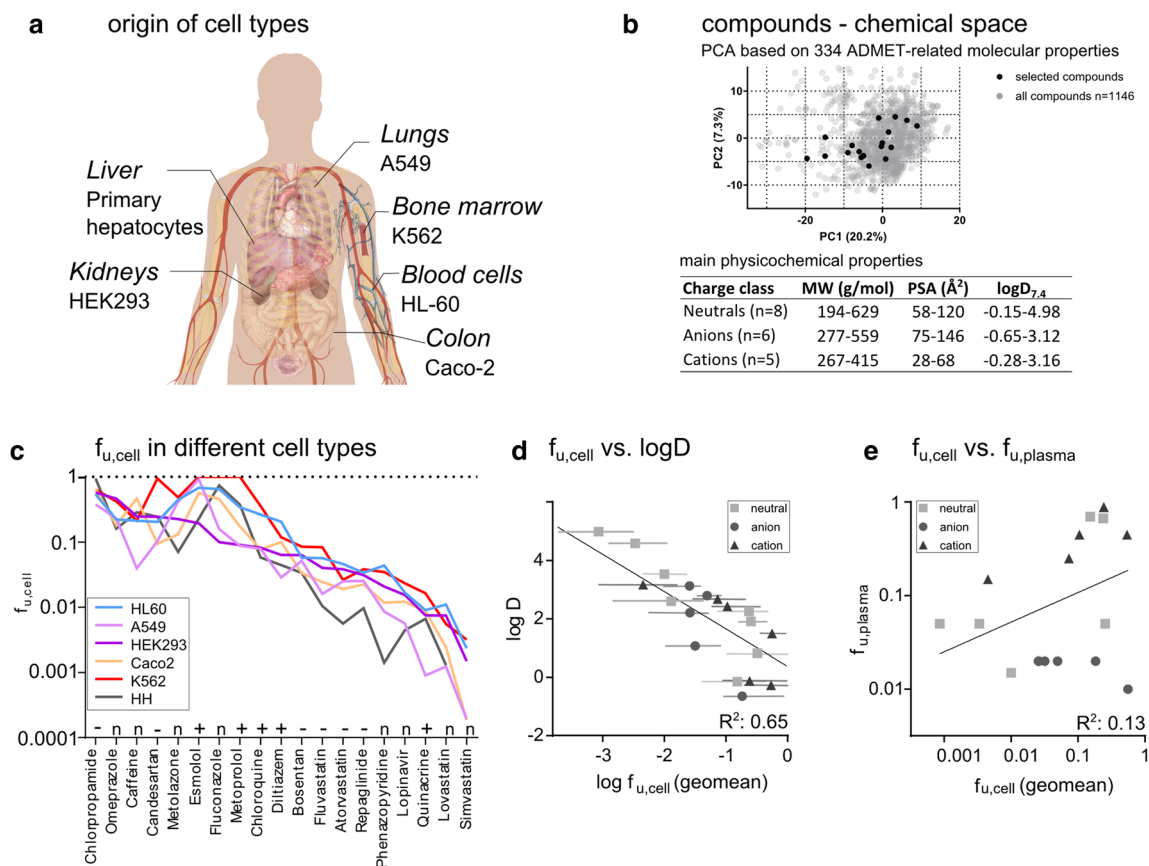
Fig. 1 (**a**) Origin of the cell types tested. (**b**) Selection and properties of compounds tested (for compounds and compound properties see Table S1 and Fig. S2). (**c**) Overview of $f_{u,cell}$ across the human cell types, sorted by decreasing $f_{u,cell}$ in HEK293 cells. For simplicity in the presentation, only geometric mean values without standard deviations are shown. Full information is available in Table S4. (**d**) Geometric mean of $f_{u,cell}$ of each compound across all cell types plotted against logD. Lines indicate maximum and minimum values of $f_{u,cell}$ (**e**) Geometric mean of $f_{u,cell}$ of each compound across all cell types plotted against $f_{u,plasma}$ derived from DrugBank (15).

significance was assessed from the linear regression of log $f_{u,cell}$ *versus* PL content (Fig. 2b). $f_{u,cell}$ was negatively correlated to the PL content in these cells, with statistical significance for four compounds (lovastatin, phenazopyridine, atorvastatin and repaglinide; $p < 0.05$). These compounds are highlighted in Fig. 2c. All 12 compounds with an $f_{u,cell}$ below 0.1 (i.e. compounds that are bound more than 90%), had slopes following the same trend. The seven low binding compounds with $f_{u,cell}$ above 0.1 (shown in grey, Fig. 2b) were not affected by PL content. Together, these results support the hypothesis that PL content is a significant contributor for unspecific cellular binding of drugs, except when the overall binding to cell membranes is low.

$f_{u,cell}$ in Comparison to Lipid Affinities

Next, we investigated if the differences in $f_{u,cell}$ could be further explained by the drug's affinity to different PL subspecies. We therefore measured affinities of the 19 compounds to beads coated with pure PC, PE or PS membranes (Fig. 3a). These three PL subspecies were chosen because they are the major PL subspecies in a mammalian cell (Fig. 3b). We also

aimed to use pure PI, but this was not possible due to the high cost of this PL. Affinities to these membranes (expressed as membrane:buffer distribution coefficients) were converted to $f_{u,PL}$ (termed specifically $f_{u,PC}$, $f_{u,PE}$ and $f_{u,PS}$ for each PL subspecies) using Eqs. 4 and 6. We observed a clear relationship of $f_{u,PL}$ to log D for the neutral compounds (Fig. 3a). This trend was less apparent for the anionic and cationic compounds, which indicates the importance of charge interactions between the drug molecules and PL membranes. All $f_{u,PE}$ values were confined within one order of magnitude ($0.01 > f_{u,PE} > 0.001$), except for the most lipophilic compound in the series (simvastatin, $f_{u,PE} = 0.0001$). The $f_{u,PC}$ and $f_{u,PS}$ values covered more evenly the range from 0.0001 to 0.05.

Next, we devised mixed beads containing all four major PL subspecies (52:22:12:14 mol% for PC:PE:PS:PI) to mimic the PL composition in a typical mammalian cell (17) (Fig. 3b). We compared $f_{u,PC}$, $f_{u,PE}$ and $f_{u,PS}$ to the $f_{u,mixed\ beads}$ to better understand the individual contribution of the PL subspecies to drug binding. To our satisfaction, drug affinities for PC, PE and PS were additive, i.e. the sum corresponded to the drug affinities for the mixed beads—provided that proportions of the individual PLs in the beads were considered. This is
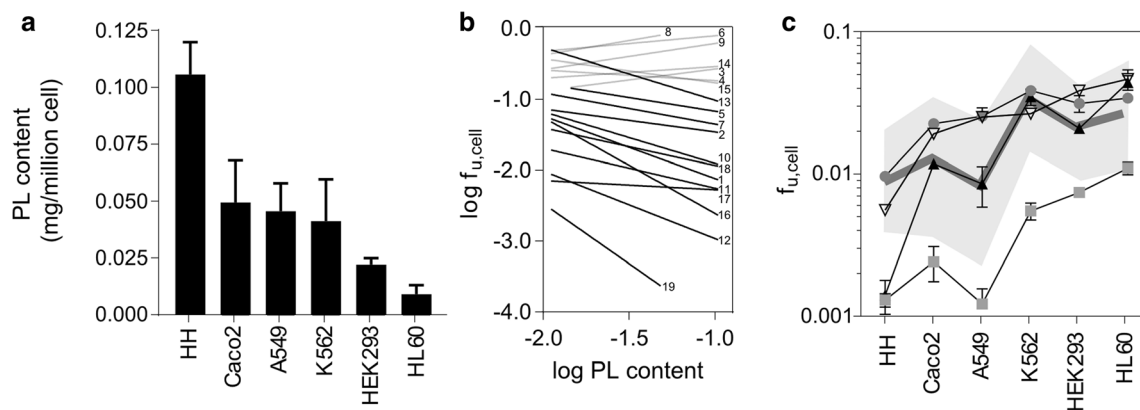
Fig. 2 (**a**) PL content (mg/million cell) determined using an enzymatic assay for each of the human cell types. (**b**) Linear regression of $f_{u,cell}$ and PL content. The numbers correspond to the compounds in Table S4. Compounds of the highly bound class ($f_{u,cell} < 0.1$, $n = 12$) are depicted in black and low binding drugs ($n = 7$) are depicted in grey. (**c**) $f_{u,cell}$ of significantly correlated compounds in panel B (lovastatin (■), phenazopyridine (▲), atorvastatin (▽) and repaglinide (●) in all human cell types, sorted according to their PL content in panel A. The thick line represents the geometric mean of $f_{u,cell}$ across all compounds in a given cell line, and the greyed area to the 95% confidence interval.

exemplified for three compounds in Fig. 3c. In this way, the drug affinities to mixed beads could be predicted from the

individual drug affinities with an average error of 1.6-fold ($R^2 = 0.83$; RMSE = 0.2; Fig. 3d).
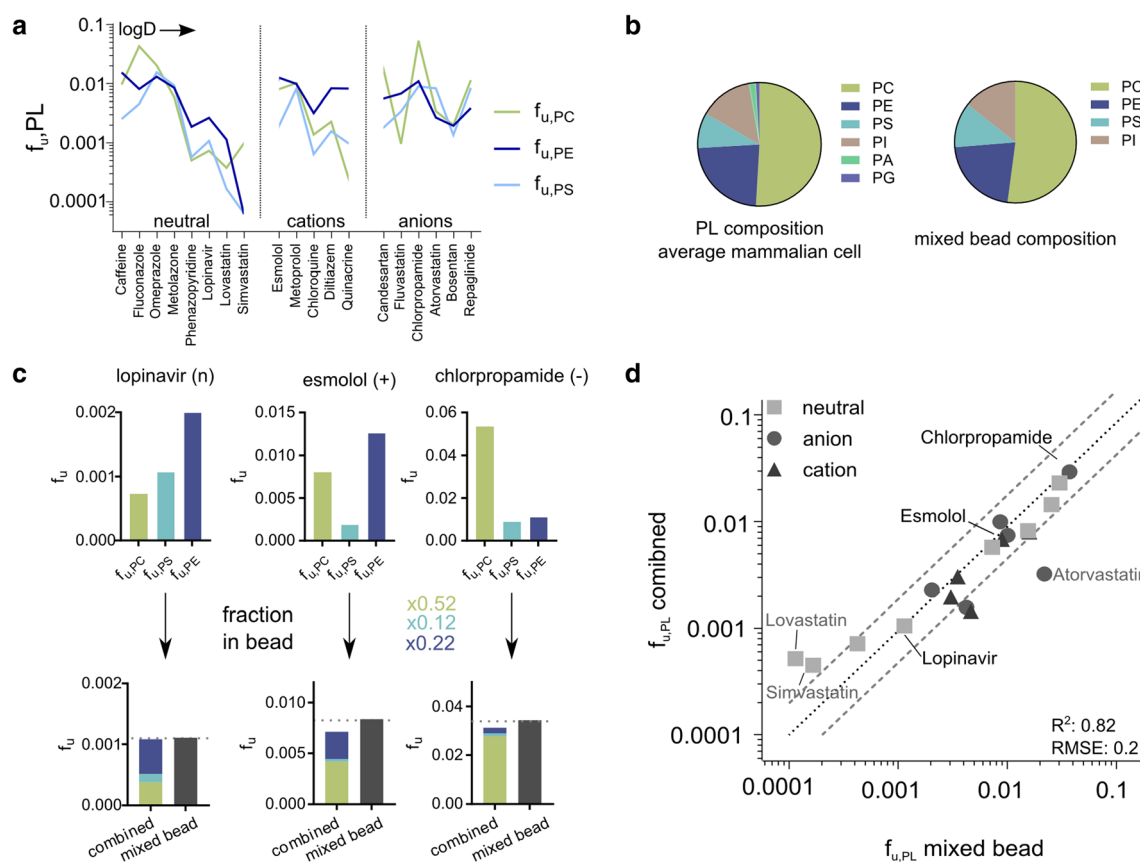

Fig. 3 (**a**) $f_{u,PC}$, $f_{u,PE}$ and $f_{u,PS}$ sorted by logD and charge class of the compounds. Numerical values are presented in Table S5. (**b**) Composition in mol% of each PL subspecies of a typical mammalian cell (17) and in the mixed beads. (**c**) Examples illustrating the additivity of drug affinities. The affinities of the individual PLs (upper panel) were multiplied with the specific fraction in the bead (0.52 for PC, 0.12 for PS and 0.22 for PE) to obtain the combined PL affinity which was compared to the one obtained in mixed beads (lower panel). Lopinavir represents a neutral compound with low $f_{u,PL}$, esmolol a cation with intermediate $f_{u,PL}$ and chlorpropamide an anion with high $f_{u,PL}$. (**d**) Correlation between drug affinities measured in beads containing a combination of lipid species ($f_{u,PL}$ mixed bead) and drug affinities calculated by combining affinities to beads containing the individual lipid species PC, PE or PS. The dotted lines indicate a 2-fold error.

To better understand the contribution of individual PLs in the cell types, we determined the proportional content of each PL subspecies for each of the 8 cell types in this study, using an MS-based shotgun approach. The total intensities of each specific PL-fragment were expressed as the percentage of the total intensities of all detected PL (Fig. 4). Since PC and sphingomyelins (SM) share the same fragment, these two lipid classes were not possible to separate without an additional ion-mobility separation technique not available in our laboratory. Based on literature data of SM abundance in mammalian cells we therefore subtracted an average content of 10% SM to calculate the percentage of PCs (17–19). Overall, our results reflected average literature values for PC (49-62%), PE (12-29%), PS (3-9%), PI (4-7%), with only minor contributions from phosphatidylglycerol (PG) and phosphatidic acid (PA).

We next used the PL composition of the cells to scale $f_{u,PL}$ to $f_{u,cell}$. The scaling was first performed by applying Eqs. 2 and 6 and an optimized dilution factor, D_L, that was determined for each cell type individually (Fig. 5a). This dilution factor represents the concentration of 'binding sites' in a Langmuir binding isotherm model. The scaling was performed separately for $f_{u,PC}$, $f_{u,PE}$, $f_{u,PS}$ and $f_{u,mixed\ bead}$. Given the observed additivity of membrane affinities (Fig. 3), we also combined the affinities obtained with beads coated with single PL-subspecies using the relative content of each PL subspecies (last panel in Fig. 5a). On the basis of R^2 and RMSE (Fig. S7), the best correlations for the different cell types were, in most cases, obtained with the mixed beads (Fig. 5b).

DISCUSSION

Structurally different drugs bind to cellular constituents such as lipids and proteins to varying degrees. This reduces the concentration of free drug available ($f_{u,cell}$) for intracellular target interactions. Because measurement of cell- and tissue-specific drug binding requires invasive methodologies, the free plasma concentration has traditionally been used as a surrogate for the free tissue concentration in specific organs. However, the correlation between these two parameters is poor and therefore methods have been developed for

measuring tissue-specific free concentrations (20,21). We have adapted one such methodology (22) to a format suitable for drug discovery applications (5,16).

Here, we use our small-scale, high-throughput method for determination of $f_{u,cell}$ to systematically investigate the unbound fraction of drugs in cells ($f_{u,cell}$) (Fig. 1a–c).

Our study indicates a significant variation of $f_{u,cell}$ across six cell types. The difference in $f_{u,cell}$ of 19 chemically diverse drugs was on average 9.5-fold for the human cell types (Fig. 1c) and correlates with total PL content in the cells (Fig. 2). Statistical analysis of the variance of a given compound between the six cell types derived from different organs and the three kidney-derived cell types from different species indicated significantly higher inter-organ variability than inter-species variability ($p = 0.0001$, paired t-test, S1). This is in line with previous studies that indicate low inter-species variability of drug binding in hepatocytes or brain tissue (9,23).

The correlation of $f_{u,cell}$ across cell types with logD (Fig. 1d) was also in-line with previous findings (5). Indeed, current in silico models for prediction of $f_{u,cell}$ rely on this parameter (24). However, the correlation with lipophilicity did not explain the spread of maximal and minimal $f_{u,cell}$ values for a given compound in the different cell types (Fig. 1d). Instead, this spread was explained by the PL concentration. Thus, cells with the highest PL content (HH) had the lowest $f_{u,cell}$ values and the cells with the lowest PL (HL60) contents had high $f_{u,cell}$ values (Fig. 2).

In this study, $f_{u,cell}$ was determined using the binding method in cell homogenates at a cell concentration of 10 million cells/ml. At this concentration, accurate determination of $f_{u,cell}$ (accepting an error of 15%) is possible for $f_{u,cell}$ values below 0.1. (16,23). For $f_{u,cell}$ values above 0.1, gradually larger errors are obtained. If desired, this error can be reduced by increasing the cell concentration (23). This is because the experimental error deceases with decreasing dilution of the cells (represented by the dilution factor D_P in Eq. 2). In our set-up, D_P is determined from protein measurements in each experiment, to account for experimental variation in cell number and differences in cell volume between different cell types. After normalization for cell number and volume, we still observe differences in binding among the various cell types, throughout the whole range of $f_{u,cell}$-values (0.0001 to 1, Fig.

Fig. 4 MS-based shotgun PL analysis of the six human cell types. Contents of individual PL subspecies are expressed as % of total identified PL species. PC and SM shared the same analytical fragment; an average content of 10% SM was therefore subtracted from the PC-MS signal, depicted in grey (17–19).
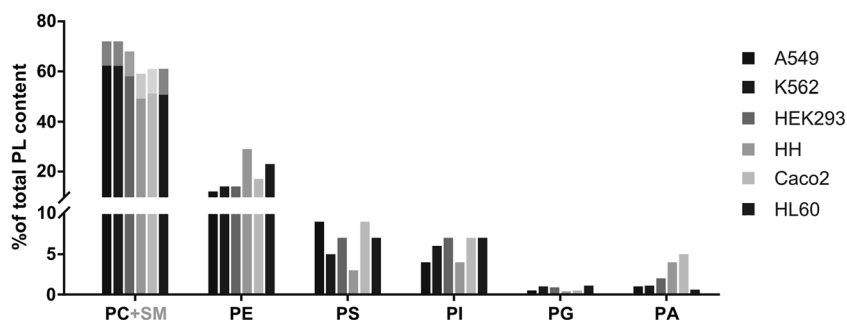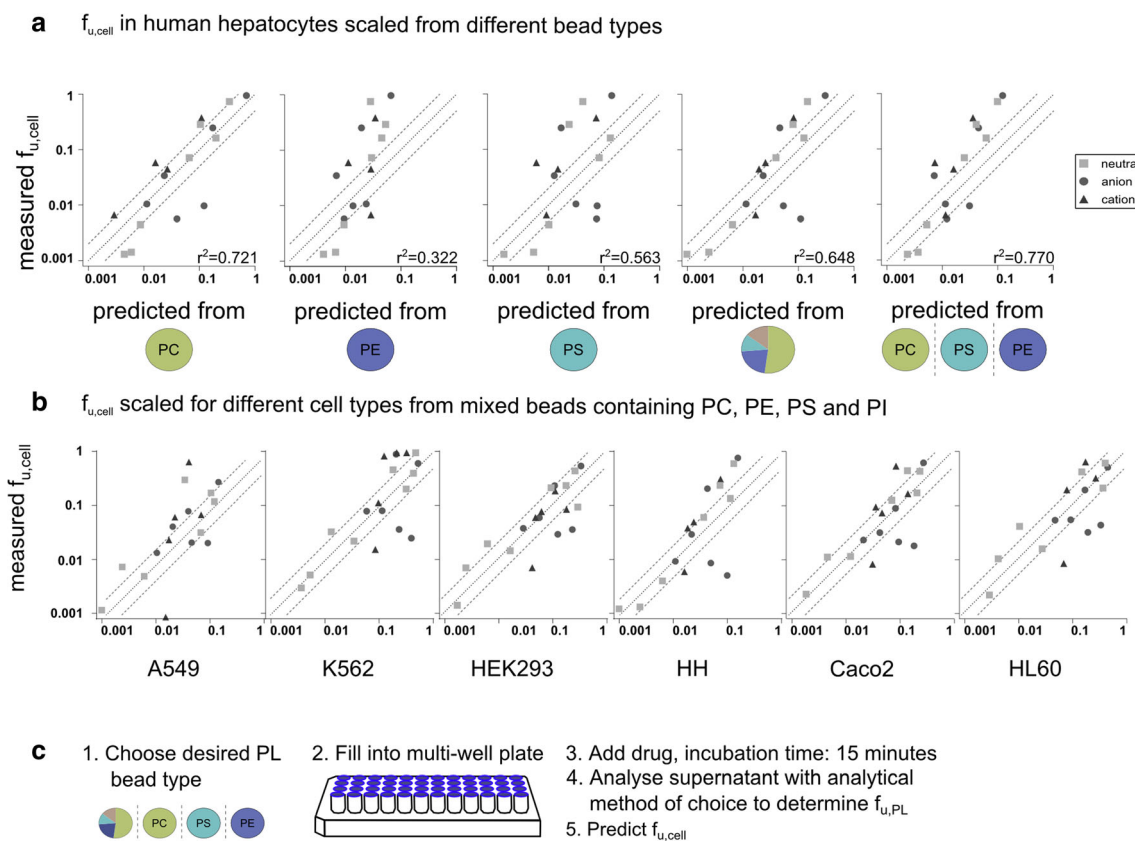
Fig. 5 (**a**) Correlations between measured and predicted $f_{u,cell}$ in human hepatocytes, based on affinities to the different bead types. The dotted line indicates a 2-fold error. A statistical overview (R^2 and RMSE) is available in S7. (**b**)). Correlation of measured and predicted $f_{u,cell}$ in the different cell types, based on the affinities to the mixed beads containing four phospholipid species (PC, PE, PS and PI). The dotted line indicates a 2-fold error. A statistical overview (R^2 and RMSE) is available in S7. (**c**) Method overview for prediction of $f_{u,cell}$ using PL beads.

1c). Therefore, we conclude that the differences of $f_{u,cell}$ between cell types is not explainable merely by dilution effects, as recently suggested (23).

A second dilution factor, D_L, that accounts for differences in binding capacity among the different cell types, was used to scale $f_{u,cell}$ from the $f_{u,PL}$ that was determined from the beads with immobilized pure PLs (Eq. 6). Cell-type specific D_L values were optimized for each PL bead type by minimizing the sum of the squared prediction errors. This approach has been used previously to predict $f_{u,brain}$ from binding to cellular homogenates (9). The optimized D_L values from the mixed PL beads were in good agreement with the D_L values that took the proportional content of PL subspecies into account. This reflects the additive properties of the bead affinities (Table S8). In line with our hypothesis that PLs are the major binding site of drugs, we observed that HH, which had the highest PL content, had the lowest D_L.

For most cell types, the best correlations with a single PL species were obtained with PC (Fig. S7). This was not surprising, given that PC is by far the most abundant PL species in cellular membranes (>50%, Fig. 4). An exception was the Caco-2 cell line, for which the best correlation was with $f_{u,PS}$ (Fig. S7). Interestingly, this cell line had one of the highest PS

contents (~9%). Previous studies on drug interactions with pure PLs indicate that binding affinities of amine-containing basic compounds can be more than hundred fold higher for PS than for PC (25). Thus, despite its lower abundance, the PS content may influence overall binding more than might be expected on the basis of its membrane concentration. However, the results in the Caaco-2 cells were not in agreement with those in A549 cells, that also had a high PS content. Factors not covered in this investigation could contribute to these differences. These include contributions from other PL-derived lipid species or differences in subcellular or even local membrane distribution of the different PL species. Cellular components not yet considered could also contribute to the discrepancy, e.g. glycogen depots that increase with time in long term cultures of Caco-2 cells. The affinity of the different drugs to PE was confined within a fairly narrow range (1 log unit, Fig. 3a) except for of the most lipophilic drug of the data set (simvastatin). Thus, the discriminative power of pure PE was low, and the values scaled from $f_{u,PE}$ gave the poorest correlations with $f_{u,cell}$ (Fig. S7).

The best correlations between binding in cells and binding to PL-coated beads were obtained when contributions from several PL subspecies were combined (Fig. 5b). However, in

this system, the $f_{u,cell}$ of three compounds (atorvastatin, repaglinide and quinacrine) was consistently over-predicted. This could not be explained by common physicochemical properties or PL affinity. Further studies are required to explain these results.

The PL profiling did not reveal any outlier in PL composition between the cell types. Similar standard culture conditions were used throughout, and it is widely recognized that membrane compositions of cells are affected by culture conditions (19,26). Therefore, PL content is likely to differ to a larger extent in primary cells that require specialized culture media developed to better reflect their tissue-specific environments. Variation in lipid composition in cells is also associated with diseased states, (27) which could lead to altered drug distribution and $f_{u,cell}$. Given the complexity of the cellular lipidome (>1000 different lipid molecules in the plasma membrane alone (28)), more detailed studies are required to elucidate these issues. In this context, it is important to note that cellular proteins contribute to non-specific cellular drug binding to a much smaller extent than PLs; even in hepatocytes, where albumin is synthesized (6,29).

In summary, the cell-free approach for determination of $f_{u,cell}$ introduced in this contribution has several experimental advantages. These include a reduced equilibration time compared to the cellular assay (15 *vs.* 240 min) and the possibility to reduce the dilution factor by increasing the number of beads. A lower dilution factor will most likely reduce the experimental errors, as observed for cell homogenates (23). Further, once the correlation to the cell type of interest has been established (in terms of D_L), the same batch of PL beads can be used, reducing experimental variability. The PL bead assay can be performed at different levels of sophistication. In its simplest form, PC-beads—representing the most abundant PL species (>50%) in cells—can be used to obtain an approximation of $f_{u,cell}$. In a more advanced variation, beads can be constructed that are composed of the most abundant PLs in proportions representing an average or a specific human cell, as exemplified by the mixed PL beads in this study. However, this approach will require custom-made beads for each cell type. As a more flexible alternative, a series of PL-beads representing each of the most common PLs can be constructed and then combined in proportions representing different cell types. Further optimization will be possible, e.g. by incorporation of cholesterol as a major membrane component, and by deconvolution of subcellular PL distribution. Our results show that $f_{u,cell}$ can be predicted by distribution into phospholipid beads. This raises the question if a cell free methodology also can be devised for determination of Kp. However, this will probably be more difficult since Kp is influenced by (sometimes unknown) cell dependent mechanisms such as active uptake and efflux transport and metabolic processes that will be difficult to mimic in a cell-free system.

CONCLUSION

In conclusion, our results indicate that, independently of cell type, the cellular PL content determines to a large extent the free cellular fraction of drugs available for interaction with intracellular targets. The PL content and composition differ between cell types and correlate to $f_{u,cell}$. We also found that $f_{u,cell}$ determined in cell homogenates can be predicted from drug affinities to PL membranes when appropriate dilution factors are applied. We therefore devised PL-covered beads that better represent the cellular contents than beads containing merely PC. These beads are a promising approach for a high-throughput and cell-free prediction of $f_{u,cell}$.

REFERENCES

1. Guo Y, Chu X, Parrott NJ, Brouwer KLR, Hsu V, Nagar S, Matsson P, Sharma P, Snoeys J, Sugiyama Y, Tatosian D, Unadkat JD, Huang SM, Galetin A. International transporter C. Advancing Predictions of Tissue and Intracellular Drug Concentrations Using In Vitro, Imaging and PBPK Modeling Approaches. Clin Pharmacol Ther. 2018.

2. Chu X, Korzekwa K, Elsby R, Fenner K, Galetin A, Lai Y, et al. Intracellular drug concentrations and transporters: measurement, modeling, and implications for the liver. Clin Pharmacol Ther. 2013;94(1):126–41.

3. Guo Y, Chu X, Parrott NJ, Brouwer KLR, Hsu V, Nagar S, et al. Advancing predictions of tissue and intracellular drug concentrations using in vitro, imaging and physiologically based pharmacokinetic modeling approaches. Clin Pharmacol Ther. 2018;104(5): 865–89.

4. Riede J, Camenisch G, Huwyler J, Poller B. Current in vitro methods to determine hepatic Kpuu: a comparison of their usefulness and limitations. J Pharm Sci. 2017;106(9):2805–14.

5. Mateus A, Matsson P, Artursson P. Rapid measurement of intracellular unbound drug concentrations. Mol Pharm. 2013;10(6): 2467–78.

6. Treyer A, Mateus A, Wisniewski JR, Boriss H, Matsson P, Artursson P. Intracellular drug bioavailability: effect of neutral lipids and phospholipids. Mol Pharm. 2018;15(6):2224–33.

7. Vildhede A, Wisniewski JR, Noren A, Karlgren M, Artursson P. Comparative proteomic analysis of human liver tissue and isolated hepatocytes with a focus on proteins determining drug exposure. J Proteome Res. 2015;14(8):3305–14.

8. Lecluyse EL, Alexandre E. Isolation and culture of primary hepatocytes from resected human liver tissue. Methods Mol Biol. 2010;640:57–82.

9. Mateus A, Matsson P, Artursson P. A high-throughput cell-based method to predict the unbound drug fraction in the brain. J Med Chem. 2014;57(7):3005–10.

10. Gillen CM, Forbush B III. Functional interaction of the K-Cl cotransporter (KCC1) with the Na-K-Cl cotransporter in HEK-293 cells. Am J Phys Cell Phys. 1999;276(2):C328–36.

11. Matyash V, Liebisch G, Kurzchalia TV, Shevchenko A, Schwudke D. Lipid extraction by methyl-tert-butyl ether for high-throughput lipidomics. J Lipid Res. 2008;49(5):1137–46.

12. Nakanishi H, Ogiso H, Taguchi R. Qualitative and quantitative analyses of phospholipids by LC–MS for lipidomics. In. Lipidomics: Springer; 2009. p. 287-313.

13. Wu Z, Shon JC, Liu KH. Mass spectrometry-based lipidomics and its application to biomedical research. J Lifestyle Med. 2014;4(1): 17–33.

14. Baker PR, Armando AM, Campbell JL, Quehenberger O, Dennis EA. Three-dimensional enhanced lipidomics analysis combining UPLC, differential ion mobility spectrometry, and mass spectrometric separation strategies. J Lipid Res. 2014;55(11):2432–42.

15. Law V, Knox C, Djoumbou Y, Jewison T, Guo AC, Liu Y, et al. DrugBank 4.0: shedding new light on drug metabolism. Nucleic Acids Res. 2014;42(Database issue):D1091–7.

16. Mateus A, Treyer A, Wegler C, Karlgren M, Matsson P, Artursson P. Intracellular drug bioavailability: a new predictor of system dependent drug disposition. Sci Rep. 2017;7:43047.

17. Vance JE. Phospholipid synthesis and transport in mammalian cells. Traffic. 2015;16(1):1–18.

18. Kurumi Y, Adachi Y, Itoh T, Kobayashi H, Nanno T, Yamamoto T. Novel high-performance liquid chromatography for determination of membrane phospholipid composition of rat hepatocytes. Gastroenterol Jpn. 1991;26(5):628–32.

19. Sampaio JL, Gerl MJ, Klose C, Ejsing CS, Beug H, Simons K, et al. Membrane lipidome of an epithelial cell line. Proc Natl Acad Sci. 2011;108(5):1903–7.

20. Hammarlund-Udenaes M. Microdialysis as an important technique in systems pharmacology-a historical and methodological review. AAPS J. 2017;19(5):1294–303.

21. Friden M, Ducrozet F, Middleton B, Antonsson M, Bredberg U, Hammarlund-Udenaes M. Development of a high-throughput brain slice method for studying drug distribution in the central nervous system. Drug Metab Dispos. 2009;37(6):1226–33.

22. Friden M, Gupta A, Antonsson M, Bredberg U, Hammarlund-Udenaes M. In vitro methods for estimating unbound drug concentrations in the brain interstitial and intracellular fluids. Drug Metab Dispos. 2007;35(9):1711–9.

23. Riccardi KA, Ryu S, Lin J, Yates P, Tess DA, Li R, Singh D, Holder BR, Kapinos B, Chang G. Comparison of species and cell-type differences in fraction unbound of liver tissues, hepatocytes and cell-lines. Drug Metab Dispos. 2018:dmd. 117.079152.

24. Kilford PJ, Gertz M, Houston JB, Galetin A. Hepatocellular binding of drugs: correction for unbound fraction in hepatocyte incubations using microsomal binding or drug lipophilicity data. Drug Metab Dispos. 2008;36(7):1194–7.

25. Murakami T, Yumoto R. Role of phosphatidylserine binding in tissue distribution of amine-containing basic compounds. Expert Opin Drug Metab Toxicol. 2011;7(3):353–64.

26. Glaser M, Ferguson KA, Vagelos PR. Manipulation of the phospholipid composition of tissue culture cells. Proc Natl Acad Sci U S A. 1974;71(10):4072–6.

27. Weijers RN. Lipid composition of cell membranes and its relevance in type 2 diabetes mellitus. Curr Diabetes Rev. 2012;8(5):390–400.

28. Escriba PV, Gonzalez-Ros JM, Goni FM, Kinnunen PK, Vigh L, Sanchez-Magraner L, et al. Membranes: a meeting point for lipids, proteins and therapies. J Cell Mol Med. 2008;12(3):829–75.

29. Wisniewski JR, Vildhede A, Noren A, Artursson P. In-depth quantitative analysis and comparison of the human hepatocyte and hepatoma cell line HepG2 proteomes. J Proteome. 2016;136:234–47.